Petroleum Science 23 (2026) 2833–2845

Contents lists available at ScienceDirect

Petroleum Science

journal homepage: www.keaipublishing.com/en/journals/petroleum-science

Original Paper

Oxidative cracking performance of low maturity shales at different O_2 concentrations

Tao Wan [a,*], Xiao Zhang [b], Ji-Xiang He [c], Yan Dong [c]

[a] Faculty of Petroleum, China University of Petroleum (Beijing) at Karamay, Karamay, 834000, Xinjiang, China
[b] PetroChina Changqing Oilfield Company, Xi'an, 710018, Shaanxi, China
[c] Exploration and Development Research Institute, Xinjiang Oilfield Company, Karamay, 834000, Xinjiang, China

ARTICLE INFO

Article history:
Received 11 October 2025
Received in revised form
27 December 2025
Accepted 31 December 2025
Available online 3 January 2026

Edited by Yan-Hua Sun

Keywords:
Low maturity shale oil
Oxidative cracking
Mechanical behavior
Oil yield

ABSTRACT

Conventional in-situ conversion technologies including electrical heating or injection of hot fluid face development challenges. Low heat transfer efficiency and limited pore expansion restrict its wide applications. Maintaining uniform heat propagation in heterogeneous shale formations remains problematic. This study investigates the cracking behavior of low-maturity organic-rich shales under inert (N_2) and oxidative (air) atmospheres, aiming to evaluate the effects of oxygen participation on reaction kinetics, pore structure evolution, and oil yield efficiency. Using integrated characterization techniques—including thermogravimetry (TG/DSC), X-ray diffraction (XRD), nitrogen adsorption–desorption, nuclear magnetic resonance (NMR), and scanning electron microscopy (SEM)—the authors demonstrate that oxidative pyrolysis significantly alters shale transformation pathways. Key findings reveal that oxygen shifts kerogen cracking to lower temperatures and enhances pore development through oxidative consumption of residual carbon, which promotes micropore expansion and connectivity, ultimately increasing total porosity by 18.9% at 600 °C. Oil yield experiments show peak production at 450 °C in air, attributed to accelerated organic matter conversion, while higher temperatures (>500 °C) trigger secondary cracking that reduces yields. These results highlight the potential of controlled oxidative pyrolysis for improving in-situ shale oil recovery efficiency while minimizing energy consumption.

1. Introduction

1.1. Status on pore structure evolution during shale pyrolysis

The development of low-maturity shale oil resources through in-situ conversion technologies faces significant challenges, including inefficient heat transfer and limited pore expansion in heterogeneous formations. Conventional thermal recovery methods, such as electrical heating or hot fluid injection, often struggle with uneven heat propagation, leading to incomplete hydrocarbon release (Sun et al., 2019). Recent studies suggest that oxidative pyrolysis—where oxygen participates in kerogen cracking—could enhance reaction kinetics and pore development compared to inert pyrolysis (Xu et al., 2021). However, the mechanisms governing pore evolution and oil yield under varying oxygen concentrations remain poorly understood.

Organic-rich shales undergo complex physicochemical reactions during pyrolysis process, where dynamic evolution of pore structure and permeability critically governs heat transfer efficiency and product migration (Gao et al., 2020; Guan et al., 2022). Kerogen embedded within the shale matrix requires hydraulic fracturing for effective pyrolysis. Nevertheless, even with artificially induced fracture networks, residual carbon from aromatics pyrolysis accumulates near wellbores limits hydrocarbons flow (Tang et al., 2025). It causes significant thermal resistance impeding heat penetration, and pore-throat blockage severely restricting hydrocarbon release efficiency (Sun et al., 2019).

During the pyrolysis of organic shales, temperature variations induce complex chemical reactions and mineral transformations within shales (Han et al., 2006). Temperature-driven

* Corresponding author.
E-mail address: 2017592002@cupk.edu.cn (T. Wan).
Peer review under the responsibility of China University of Petroleum (Beijing).

https://doi.org/10.1016/j.petsci.2025.12.041

physicochemical transformations of organic matter and minerals profoundly alter petrophysical properties (Meng et al., 2024; Rabbani et al., 2017). Upon heating, shale oil initially generates pyrobitumen as the primary product. This viscous substance fills existing pores, causing a significant reduction in porosity compared to the pre-heated samples (Fang et al., 2012). During conventional pyrolysis, below 300 °C, thermally induced microcracks dominate (Liu et al., 2022; Yang et al., 2016). Between 300 and 520 °C, kerogen pyrolysis and mineral decomposition drive substantial pore volume expansion. However, at this stage, bitumen undergoes condensation reactions while transforming into hydrocarbons (Zhan et al., 2022). These reactions produce non-hydrocarbon compounds (e.g., coke) that partially obstruct pores, resulting in renewed porosity reduction. Above 520 °C, carbonate dissolution and mineral framework fracturing further promote macropore generation. Thus, the evolution of pore structure during shale oil pyrolysis is indeed highly complex, driven by interdependent physicochemical transformations across multiple scales.

1.2. Evolution and characterization of pore structure of shales

Different experimental techniques have revealed the multi-scale characteristics of pore and permeability evolution during the pyrolysis of organic-rich shales (Lei et al., 2021). Yang et al. (2016) analyzed the pore structure evolution of organic-rich shale after pyrolysis at different heating temperatures based on high-pressure mercury injection experiments. It found that an increase in final pyrolysis temperature is usually accompanied by an increase in total pore volume, average pore size, and porosity. Nuclear magnetic resonance experiments show that when the pyrolysis temperature increases from 100 to 700 °C, the pore size distribution of organic-rich shales shows significant stage differences (Hao et al., 2016).

Low-temperature nitrogen adsorption–desorption experiments show that the specific surface area and total pore volume during pyrolysis show a nonlinear trend of first decreasing and then increasing (Bai et al., 2012; Chen et al., 2018; Han et al., 2006). X-ray computed tomography (CT) scanning technology visually presents the three-dimensional expansion process of the internal pore and fracture network of shales. At 100–300 °C, primary bedding fractures develop along the edges of minerals, and after 300 °C, kerogen cracking drives the proliferation and interconnection of fractures. Between 400 and 500 °C during the transformation of organic matter within laminations, localized fracture networks develop and porosity increases, forming connected channels mainly along the layered structure. At 600 °C, dispersed pore clusters are completely connected (Saif et al., 2017; Tiwari et al., 2013).

Research also indicates that external conditions (such as injection pressure and heating rates) have a regulatory effect on pore structure: under constant pressure, the total pore volume, specific surface area, porosity, and effective porosity of organic-rich shales all increase with the rise of pyrolysis temperatures (Bai et al., 2017; Gai et al., 2014). Meanwhile, some pores show a phenomenon of connection and merging, and the pore connectivity improves. A lower heating rate is conducive to the formation of mesopores with a pore diameter of about 3 nm, while a high heating rate may cause a sharp fluctuation in specific surface area and pore volume.

Prior research has extensively characterized pore structure evolution during inert pyrolysis, yet few studies systematically compare oxidative and non-oxidative environments. Oxygen is known to lower activation energies for kerogen cracking, but its impact on pore connectivity and secondary cracking thresholds requires further investigation. Additionally, while supercritical fluids (H_2O/CO_2) have been explored for shale pyrolysis, the role of oxygen concentration in optimizing energy efficiency and oil recovery remains unresolved.

1.3. Research status on atmosphere effects in shale pyrolysis

Pyrolysis atmosphere critically regulates reaction kinetics, product distribution, and pore evolution. In air/oxygen-rich atmospheres, pyrolysis transitions from purely thermal decomposition to a coupled oxidation-thermal process (Geng et al., 2017; Xu et al., 2021). Oxygen actively participates in pyrolysis reactions, which lower the activation energy for kerogen cracking and accelerate reaction kinetics. This creates self-sustaining exothermic reactions, significantly reducing external heating needs. Conversely, in a N_2 atmosphere, pyrolysis proceeds via thermal cracking without oxidative interference. Kerogen decomposes solely through scission of C–C and C–S bonds, driven entirely by external heat input. The absence of oxygen eliminates combustion pathways, resulting in slower, endothermic reactions that demand continuous energy supply (Gao et al., 2022; Ifticene et al., 2022).

Oxygen-rich pyrolysis amplifies pore development through dual pathways: oxidative etching of carbon residues increases microporosity, and decomposition of carbonate minerals creates larger macropores (Zhang et al., 2024). However, in a N_2 atmosphere, pore formation is primarily driven by organic volatilization, with limited mineral changes. Comparatively, high-temperature N_2 atmosphere favors reducing olefins while increasing light aromatics/alkanes, whereas CO_2 atmosphere yields lower C_{10}–C_{15} alkanes (Liu et al., 2024; Shi et al., 2024; Zhao et al., 2020).

Supercritical fluids (H_2O/CO_2) outperform inert gases (N_2) in enhancing process efficiency and product quality while significantly modifying pore structure (Wang et al., 2019; Yang et al., 2021). Supercritical water dissolves feldspars, carbonates, and pyrite via thermophysical-catalytic coupling, significantly increasing pore range while reducing sub-10 nm pores (Li et al., 2023). Compared to high-temperature nitrogen, the use of high-temperature steam significantly increases shale oil yield, attributing to steam's ability to suppress oil coking within the oil shale matrix (Meng et al., 2023). Concurrently, higher steam injection rates elevate the content of aliphatic and aromatic hydrocarbons in the oil while reducing polar compounds (Meng et al., 2024; Zhao et al., 2022).

Prior studies focus on inert pyrolysis, with limited systematic comparison of oxidative vs. inert atmospheres, especially regarding pore connectivity and secondary cracking thresholds. The role of oxygen concentration in optimizing energy efficiency and oil recovery remains unresolved. In this study, we directly contrast oxidative (air) and inert (N_2) pyrolysis using integrated techniques (TG/DSC, XRD, NMR, nitrogen adsorption) to quantify differences in reaction kinetics, pore evolution, and oil yield. The key innovation lies in demonstrating that oxygen-assisted pyrolysis significantly reduces the required reaction temperature while maintaining high oil yields, thereby offering a more energy-efficient approach for in-situ shale oil conversion. Notably, the oxidative consumption of residual carbon leads to a remarkable porosity increase, which significantly improves fluid flow characteristics. The research identifies 450 °C as the optimal temperature for peak oil yield in oxidative conditions, while also establishing the temperature threshold beyond which secondary cracking reduces oil recovery. These findings not only advance fundamental understanding of shale pyrolysis mechanisms but also have important practical implications for developing more sustainable extraction technologies. The comprehensive mechanistic insights provided in this work represent a step forward in optimizing shale

oil recovery processes while addressing environmental concerns associated with conventional thermal recovery methods.

2. Experimental methodology and procedures

In order to perform oxidative cracking experiments at different oxygen concentrations, the target shale oil cores were obtained from the Lucaogou Formation in the Junggar Basin, a typical basin containing low-maturity shale with TOC up to 18%, where immature kerogen (S_1 > 15 mg HC/g rock) generated movable hydrocarbons at R_o of 0.6%–1.2%. Sub-sampling prioritized millimeter-scale laminations using cryogenic micro-drilling to preserve kerogen distribution and natural fracture networks.

2.1. Combined TG and XRD analyses of shale oil cracking

The acquired shale samples were crushed and sieved to obtain powder with particle size of small than 200 mesh ($\Phi < 0.075$ mm), then divided into 9 groups with mass ≥0.1 g. Firstly the crushed shale samples were subject to X-ray diffraction (XRD) phase analysis experiments, at meanwhile these groups were performed to synchronous thermogravimetric/differential scanning calorimetry (TG/DSC) analysis. Prior to XRD testing, samples underwent oxidative pyrolysis pretreatment as follows: One group was randomly selected as a control group. The other six groups were uniformly distributed in batches within a muffle furnace. Under an air atmosphere (gas flow rate: 50 mL/min), samples were heated from ambient temperature to target final temperatures (100, 200, 300, 400, 500, and 600 °C) at a heating rate of 5 °C/min, followed by 4 h of isothermal holding at each target temperature.

2.2. Integrated NMR and nitrogen adsorption analyses of shale oil cracking

Standard cylindrical shale cores (Φ25 mm × 50 mm) were drilled parallel to the bedding plane, yielding a total of 12 samples. These low maturity organic-rich shale samples were divided into two groups of six each. The first group underwent pyrolysis in a muffle furnace using quartz boats under an air atmosphere (O_2 content: 21%), with samples heated from ambient temperature to target endpoints (100, 200, 300, 400, 500, and 600 °C) at 5 °C/min and a gas flow rate of 50 mL/min. Simultaneously, the second group was subjected to identical cracking conditions under a nitrogen (N_2) atmosphere. As shown in Fig. 1, oxidative cracking of samples was arranged by atmosphere: air group (Fig. 1(a)) and nitrogen group (Fig. 1(b)).

Post-cracking: Complementary application of low-field nuclear magnetic resonance (NMR) and nitrogen adsorption–desorption isotherms provides a robust framework for characterizing pore size evolution after shale oil cracking. NMR is particularly sensitive to closed pores and nanopores inaccessible to nitrogen adsorption, while also detecting fluid mobility changes during thermal maturation. Nitrogen adsorption–desorption complements NMR by precisely quantifying mesopore (2–50 nm) size distributions through Barrett–Joyner–Halenda (BJH) analysis of the adsorption hysteresis loops. During cracking, NMR detects progressive shifts in T_2 distributions toward shorter relaxation times, indicating the generation of porosity induced by thermal cracking from kerogen conversion. By cross-validating pore size distributions and reconciling discrepancies through multiphysics modeling, this dual approach effectively quantifies the cracking-driven transformation of the pore system, which is critical for predicting hydrocarbon mobility and recovery efficiency.

Fig. 1. Two groups of organic-rich shale samples cracking at air (**a**) and N_2 (**b**) conditions.

2.3. Oil yield performance of shales at N_2 and air atmospheres

Shale oil core samples are placed in a high-temperature tube furnace connected to gas supply systems, with one set exposed to pure nitrogen and another to compressed air (21% O_2), both maintained at controlled flow rates (50 mL/min) to ensure consistent atmospheric conditions. The temperature program initiates at ambient temperature with a heating ramp of 5 °C/min, progressing to target temperatures ranging from 100 to 600 °C. Samples are held isothermally at peak temperatures for 120 min to simulate in-situ conversion kinetics, during which organic matter undergoes distinct pathways: thermal cracking of kerogen into mobile hydrocarbons under N_2, versus combustion-assisted decomposition under air. During cracking, real-time monitoring tracks mass loss (thermogravimetry) and gas evolution.

To ensure the accuracy of the experimental data, cracking test measurements are repeated three times under each condition. The oil yield calculation formula for products is expressed as follows:

$$Y_o = \frac{m_l - V_w \cdot \rho}{m_s} \times 100\%$$

$$Y_w = \frac{V_w \cdot \rho}{m_s} \times 100\%$$

where Y_o is the yield of cracking oil; Y_w is the yield of pyrolysis water; m_s is the mass of organic-rich shale sample used pre-cracking, g; m_l is the total mass of liquid products, g; V_w is the volume of generated water, cm^3; ρ is the density of water, g/cm^3.

3. Results and discussion

3.1. TG-DSC and XRD analyses of shale oil cracking at N_2 and air conditions

Given the influence of mineral composition and content in organic-rich shales on pore structure evolution during cracking, X-ray diffraction analysis was conducted on these shales to precisely elucidate mineralogical evolution. Simultaneously, TG-DSC analysis was performed to further unravel the thermogravimetric behavior and energy transition characteristics during oxidative cracking processes.

Fig. 2 displays the thermal decomposition characteristics of organic-rich shales under two distinct atmospheres, with the horizontal axis representing the temperature of the internal reference within the instrument. As observed in Fig. 2, the cracking process of organic-rich shales can be divided into 3 fundamental reaction stages under both inert and oxidative atmospheres. The first stage (from ambient temperature to 290 °C) exhibits minimal mass change in the shale samples, primarily driven by the

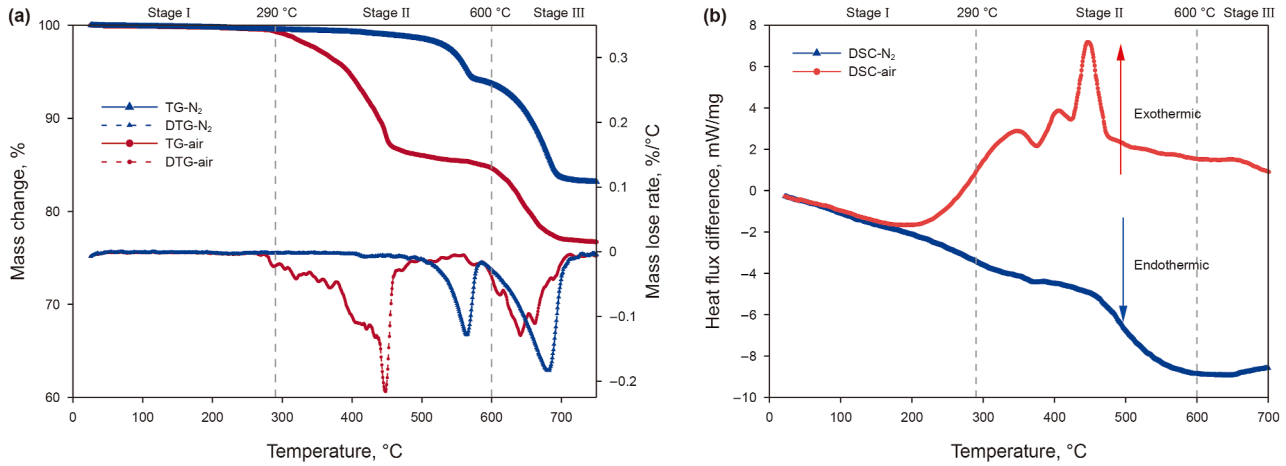

Fig. 2. Thermal decomposition characteristic curves of organic-rich shales.

evaporation of free water and adsorbed water (Zhao et al., 2025). As temperature gradually increases, interlayer water from clay minerals is progressively released, concurrently accompanied by desorption of adsorbed gases.

The second stage (290–600 °C) represents the principal thermal weight-loss interval. During this stage, organic kerogen thermally cracks into low-molecular-weight gaseous products and unstable bitumen. With further temperature elevation, this unstable pyrolytic bitumen, whose chemical structure and carbon content resemble kerogen, undergoes additional cracking. This process generates more stable pyrolytic oil, gaseous volatiles, and non-volatile carbon residues (Pan et al., 2023; Wang et al., 2016; Zhao et al., 2025).

The third stage (>600 °C) involves thermal decomposition of carbonate minerals (e.g., calcite, dolomite) and other clay minerals rather than organic matter decomposition (Jiang et al., 2024).

Mineralogical characterization of low maturity organic-rich shales was performed via X-ray diffraction spectral analysis, with diffraction peaks labeled as follows: Q (quartz), A (albite), K (potassium feldspar), C (calcite), D (dolomite), P (pyrite), I (illite), and M (montmorillonite). The mineral identification results are presented in Fig. 3.

Fig. 3 reveals a distinct attenuation of pyrite's characteristic diffraction peak intensity at 400 °C, with near-complete disappearance by 500 °C (Boyabat et al., 2004; Hu et al., 2006). Table 1 presents the minerals changes during pyrolysis at different temperatures. During the pyrolysis of shale oil at typical temperature of 100–600 °C, quartz and feldspar remains relatively stable within this temperature range. The carbonate minerals, calcite ($CaCO_3$) and dolomite, undergo thermal decomposition, releasing CO_2 gas. The most reactive mineral, pyrite, readily decomposes in the heating process, resulting in a material with significantly different chemical reactivity and physical properties compared to the raw shale. This phenomenon arises from pyrite's phase transformation and decomposition within the 400–500 °C range, where its crystal lattice progressively disintegrates, altering both physical and chemical properties. As the temperature increases, pyrite undergoes conversion to secondary mineral phases—primarily hematite (Fe_2O_3), magnetite (Fe_3O_4), iron sulfide (Fe_2S_3), and elemental sulfur (S). Notably, elemental sulfur facilitates depolymerization and cracking of kerogen macromolecules while suppressing aromatization reactions. By 500 °C, pyrite decomposition stabilizes, achieving thermodynamic equilibrium (Dunn et al., 1989).

The increase in relative content of quartz, feldspar, albite, and clay at 600 °C after oxidative cracking primarily results from the decrease in pyrite's relative proportion, as seen in Table 1. Carbonate minerals in the Lucaogou Formation shale are dominated by dolomite and calcite. XRD analysis indicates negligible content variation in carbonate minerals (dolomite/calcite) from ambient temperature to 500 °C. Only upon reaching 600 °C diffraction peaks attenuate, with calcite exhibiting more pronounced transformation (Jiang et al., 2024).

3.2. NMR characterization of shale pore structure development

NMR characterization of pore structure in organic-rich shales was performed both before and after cracking under varying atmospheric conditions, thereby enabling systematic analysis of how cracking atmospheres influence pore size distribution across multiple scales and porosity evolution within shale matrices.

Fig. 4 presents the nuclear magnetic resonance (NMR) T_2 spectra of shale samples cracking at various temperatures under inert N_2 and air atmospheres. Based on the pore classification standard, the pore size distribution intervals—classified as micropores (10–100 nm), mesopores (100–1000 nm), and macropores (>1000 nm)—are delineated in Fig. 4.

Throughout the entire cracking process, mesopores (100–1000 nm) remain dominant, with their volume fraction minimal overall variation across temperatures. The expansion stress generated by the release of light hydrocarbon gases during cracking propels pore formation and enlargement, while the removal of carbonaceous residues from pore surfaces enhances pore connectivity. This indicates that the temperature stage (300–400 °C) is critical for mesopore development. At earlier cracking phase, the evaporation of free and adsorbed water from organic-rich shale intensifies, coupled with enhanced diffusion of interlayer water in clay minerals (Pan et al., 2023; Zhao et al., 2025). These physical processes collectively promote mesopore formation and significantly restructure the pore network.

Based on the observed experimental results, it infers that the introduction of oxygen in an air atmosphere generates exothermic effects through the oxidation of residual carbon and other organic matter, as shown in Fig. 4. This process not only releases more heat than in a nitrogen environment—accelerating cracking—but also provides additional energy input for the pyrolysis of deep-seated kerogen in shale samples, thereby enhancing the depth of cracking reactions. Furthermore, the oxidative consumption of residual carbon liberates additional pore space, promoting the expansion, connectivity, and merging of micropores, ultimately facilitating their transformation into macropores, as shown in

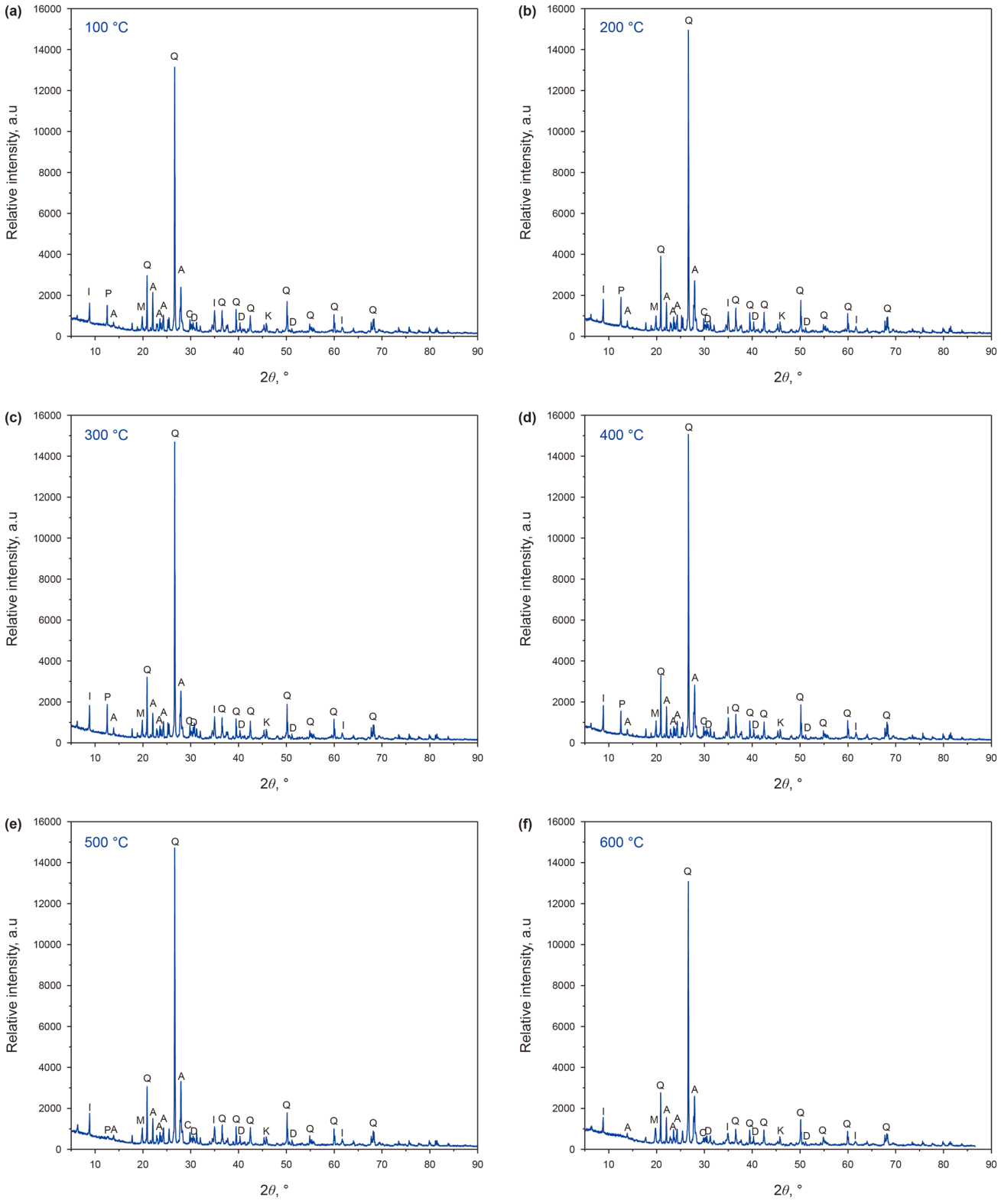

Fig. 3. XRD mineral calibration of shale samples at different cracking temperatures.

Fig. 4. Air atmosphere induces markedly accelerated and enhanced pore restructuring. Above 500 °C, oxidative pyrolysis generates a striking pore network transformation, while synergistic effects of carbon oxidation and mineral decomposition drive porosity significantly surpassing in N_2.

Fig. 5(a) demonstrates that in a N_2 atmosphere, both the proportions of micropores and mesopores gradually decrease with rising temperature. The proportion of micropores declines continuously from 21.3% at 100 °C to 13.7% at 600 °C, representing a cumulative reduction of 7.6%. Notably, 54.0% of this decrease

Table 1
Change of minerals at different pyrolysis temperatures.

Pyrolysis temperature, °C	Mineral content, %						
	Quartz	Potassium feldspar	Albite	Pyrite	Dolomite	Calcite	Clay
Raw	40.3	4.9	14.8	6.7	11.3	4.5	17.5
100	39.9	5.3	14.2	7.2	11.1	4.9	17.4
200	40.7	5.2	14.9	6.7	10.9	4.4	17.2
300	40.5	4.8	15.1	6.4	10.9	4.5	17.8
400	41.7	5.4	15.5	4.1	11.4	4.7	17.2
500	42.1	5.6	16.6	0.6	13.8	4.9	16.4
600	43.7	5.9	17.2	0.2	12.4	2.9	17.7

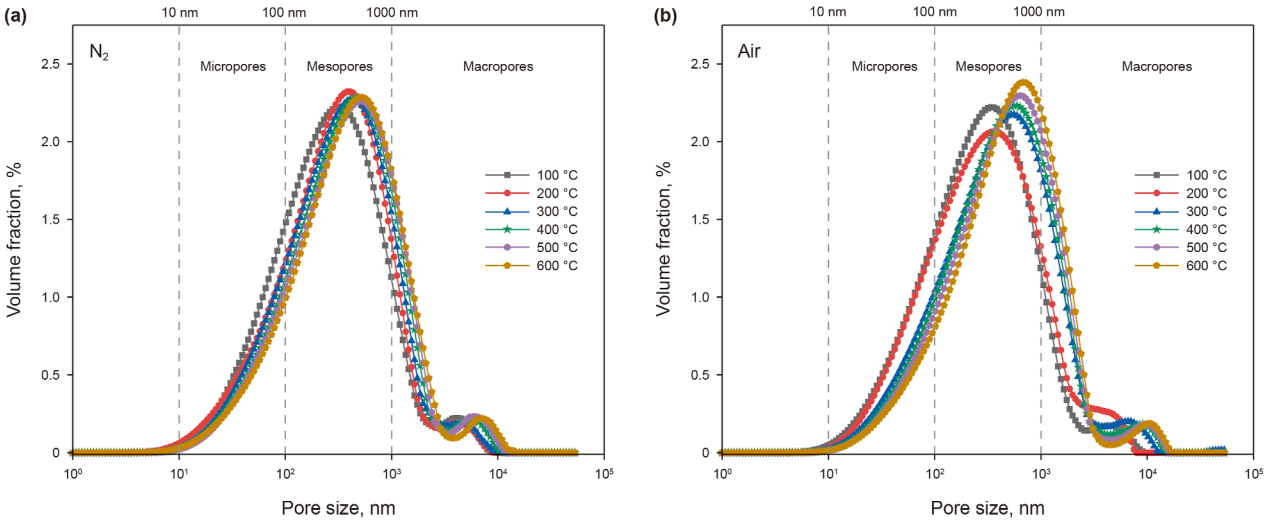

Fig. 4. Pore size distribution of shale samples at different cracking temperatures at N_2 (**a**) and air (**b**) conditions.

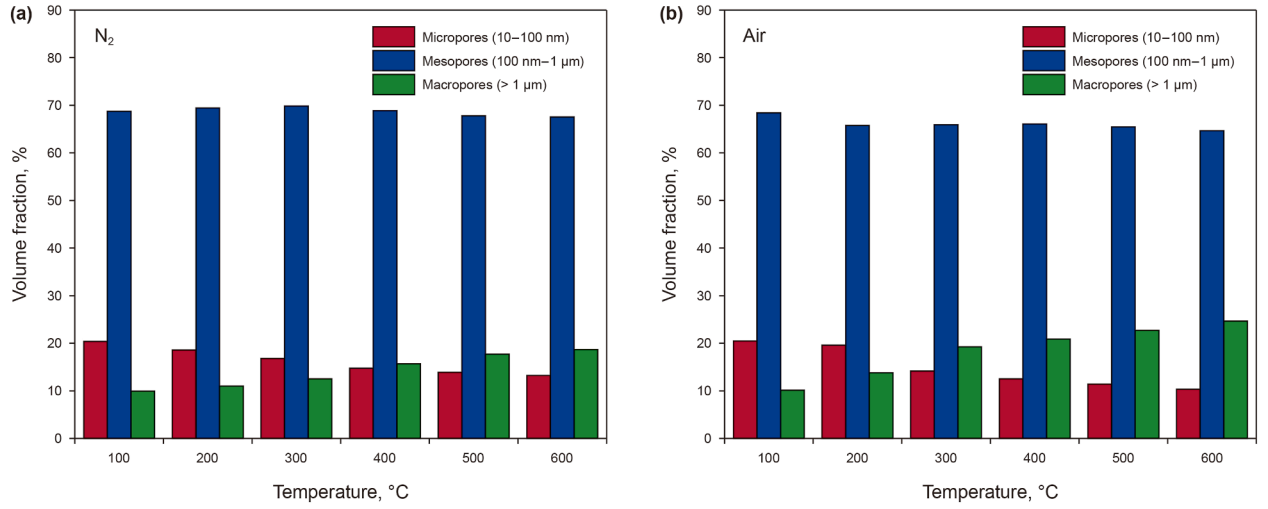

Fig. 5. Comparison of pore evolution at different N_2 (**a**) and air (**b**) heating temperatures.

occurs within the 200–400 °C interval. Within this critical temperature range, micropores and mesopores undergo substantial transformations during cracking, where mineral expansion and gas pressure from organic matter decomposition induce pore conversion to larger apertures (Guo et al., 2020).

Contrast to that, subplot of Fig. 5(b) reveals that under an air atmosphere, the combined volume fraction of the micropore distribution sharply declines from 21.46% at 100 °C to 10.69% at 600 °C, representing a cumulative reduction of 10.77%—whose reduction is larger than observed under a N_2 atmosphere. Notably, the critical temperature-responsive ranges for pore evolution differ significantly between atmospheres: Under a N_2 atmosphere, the most substantial decline in micropore occurs within the 300–400 °C interval. While under an air atmosphere, the maximum reduction manifests in the 200–300 °C range. The existence of O_2 lowers the oxidative cracking temperature for kerogen oxidation and pore structure evolution.

As shown in Fig. 6, the pore system of organic-rich shales exhibits volumetric expansion under both atmospheres with increased cracking temperatures. Under a N_2 atmosphere, porosity rises from 6.2% at 100 °C to 16.3% at 600 °C, representing an increase of 10.1%. In contrast, under an air atmosphere, it surges from 5.9% to 18.9%, much higher than that under a N_2 atmosphere. This confirms the distinct advantage of air atmosphere in promoting shale pore network development and enhancement.

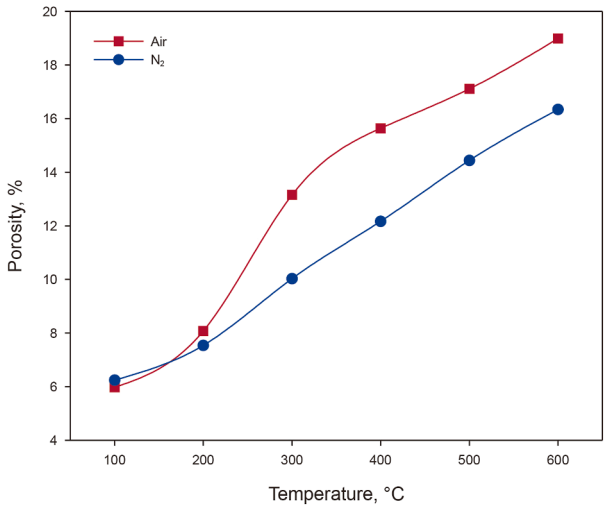

Fig. 6. Comparison of pore size distribution of shales at different cracking temperatures.

3.3. SEM characterization

The evolutionary characteristics of pore-fracture morphology on shale surfaces can be directly observed via scanning electron microscopy (SEM). Organic-rich shales contain abundant nanoscale pores. During oxidative cracking at high temperatures, thermal expansion of inorganic minerals and organic matter may induce thermal fracturing in shale, as shown in Fig. 7.

As illustrated in Fig. 7, the original organic-rich shale exhibits a solid surface structure. Observations of Fig. 7 reveal that the microstructure of surface pores shows negligible changes at lower pyrolysis temperatures (ambient temperature ~200 °C), with mineral particles tightly packed. This indicates that cracking reactions are still at initial stage, where changes are predominantly governed by physical processes, such as the release of free water, adsorbed water, and volatile organic components (Zhao et al., 2025).

Concurrently, comparative analysis with high-temperature SEM images demonstrates under a N_2 atmosphere, softening deformation becomes observable at 300 °C (Fig. 7(c)), attributed to the conversion of kerogen into bitumen. As the temperature increases to 400 °C (Fig. 7(d)), distinct cracks and fractures emerge on the surface due to violent release of pyrolytic hydrocarbons, though most pores in the shale samples remain incompletely opened (Pan et al., 2023; Jiang et al., 2024). Subsequently, at 500 °C (Fig. 7(e)), a significant increase in irregularly shaped pores occurs, accompanied by collapse and coalescence of adjacent pores. When the temperature reaches 600 °C (Fig. 7(f)), honeycomb-like, relatively ordered macropores (>1000 nm) develop across the shale surface (Guo et al., 2020; Wang et al., 2022).

In an air atmosphere, the oxidative modification of pore structure during cracking at 400–600 °C demonstrates markedly enhanced characteristics (Fig. 7). At 400 °C, the cleavage of macromolecular organics generates volatile products. Upon heating to 500 °C (Fig. 7(k)), oxidation kinetics dominate: (1) Consumption of residual carbon liberates additional pore space. (2) Localized temperature gradients by oxidation cause thermal expansion, generating secondary microfractures. (3) Stress mismatch between decomposed ferromagnesian minerals promotes the development of pore systems. At 600 °C (Fig. 7(l)), synergistic oxidation-cracking effects peak: near-complete oxidation of residual surface organics coincides with lattice destruction, resulting in interconnection and merging of isolated pore clusters into integrated networks (Dunn et al., 1989; Liu et al., 2024).

3.4. Nitrogen adsorption–desorption analysis of shale oil cracking at N_2 and air conditions

The isothermal nitrogen adsorption–desorption method is primarily used to analyze the specific surface area, total pore volume, pore size distribution, and average pore diameter in organic-rich shales. During cracking process, the pore size distribution and pore morphology of organic-rich shales significantly influence the convective heat transfer process of injected gases. Simultaneously, these parameters critically govern the seepage and escape of pyrolytic products. Therefore, elucidating the evolutionary patterns of these parameters is essential for clarifying the cracking mechanisms of organic-rich shales.

Figs. 8 and 9 present the isothermal adsorption–desorption curves of pyrolyzed shale samples under N_2 and air atmospheres, respectively, at varying final cracking temperatures.

Analysis of Fig. 8 indicates that shale samples subjected to pyrolysis at 100–600 °C under a N_2 atmosphere consistently exhibit Type II isotherm adsorption curves (Sing et al., 1985). This demonstrates that after high-temperature pyrolysis (600 °C), the internal pore structure of organic-rich shale undergoes no substantial alteration, retaining its porous characteristics. In contrast, Fig. 9 reveals that under an air atmosphere, shale samples pyrolyzed at 100–400 °C similarly display Type II isotherm curves. However, when the pyrolysis temperature reaches 500 °C, the curve morphology undergoes a marked transition to a characteristic Type III isotherm, typically associated with macroporous media. This indicates significant restructuring of the shale's microporous architecture during high-temperature oxidative cracking. The phenomenon is preliminarily attributed to oxygen-induced oxidation and consumption of residual carbon, which liberates additional pore space. Coupled with thermal expansion of gaseous oxidation byproducts under high temperatures, this process promotes the coalescence of micropores and mesopores, ultimately generating new macropores (Wang et al., 2022).

Further examination of Fig. 9 shows that the adsorption–desorption isotherms for organic-rich shale samples pyrolyzed in air between 100 and 400 °C exhibit no significant changes. However, upon increasing the temperature to 500 °C, the hysteresis loop features undergo dramatic transformation: (1) The loop separation area narrows considerably. (2) The adsorption and desorption branches become nearly parallel. (3) The inflection point on the desorption branch disappears. This shift from H3-type to H4-type hysteresis indicates that during oxidative cracking between 400 and 500 °C, the shale's pore structure transitions from narrow “parallel-plate” slit-shaped pores to open-ended wedge pores (Sing et al., 1985). In an air atmosphere, when the final pyrolysis temperature is below 300 °C, the pore size distribution shows no significant change. As seen in Fig. 10, when the temperature further reaches 500 °C, micropores smaller than 2 nm almost disappear, while mesopores in the 2–50 nm range become predominant, and macropores larger than 50 nm also begin to form. At 600 °C, the cumulative pore volume distribution curve shifts rightward along the horizontal axis compared to that at 500 °C, with further increases in the proportions of mesopores and macropores, indicating a significant expansion and reorganization of the pore structure on the shale surface during this stage.

3.5. Comparing shale oil cracking behavior at different O_2 concentrations

The study employs a designed oxidative cracking experimental apparatus to simulate the in-situ conversion process of shale oil. Experimental procedures were described in Section 2.3. By varying oxygen concentration as an influencing factor, the research

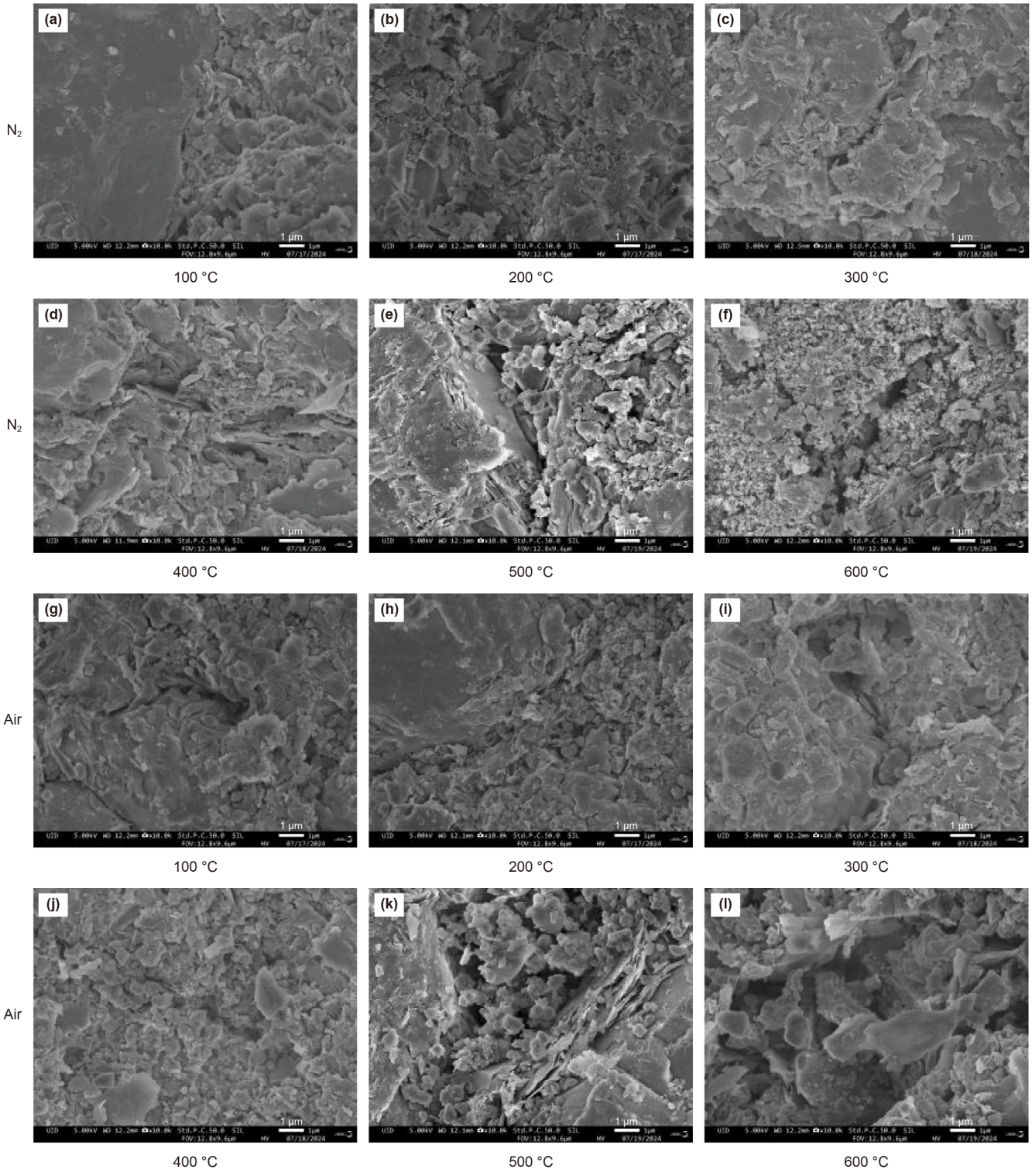

Fig. 7. Surface topology evolution of shale samples at varying conditions.

investigates how this factor influences heating rates, pressure dynamics, and oil yield during shale oil extraction. In in-situ conversion of shale oil, the oxygen concentration in injected gas is a critical determinant of reaction intensity, governing both the stability of reaction front propagation and gas sweep efficiency. As a key technical parameter for successful implementation, optimal oxygen concentration ensures controlled exothermic reactions.

Table 2 documents cracking response results under an oxygen-lean atmosphere (10% O_2/90% N_2) across 100–550 °C, quantifying mass changes in organic-rich shales. Oxidative cracking results demonstrate progressive mass loss increase from 0.05% at 100 °C to 23.72% at 550 °C.

Fig. 11 illustrates oil yield results at different pyrolysis temperatures under a N_2 atmosphere. Below 200 °C, at low-temperature conditions reactions are primarily driven by the

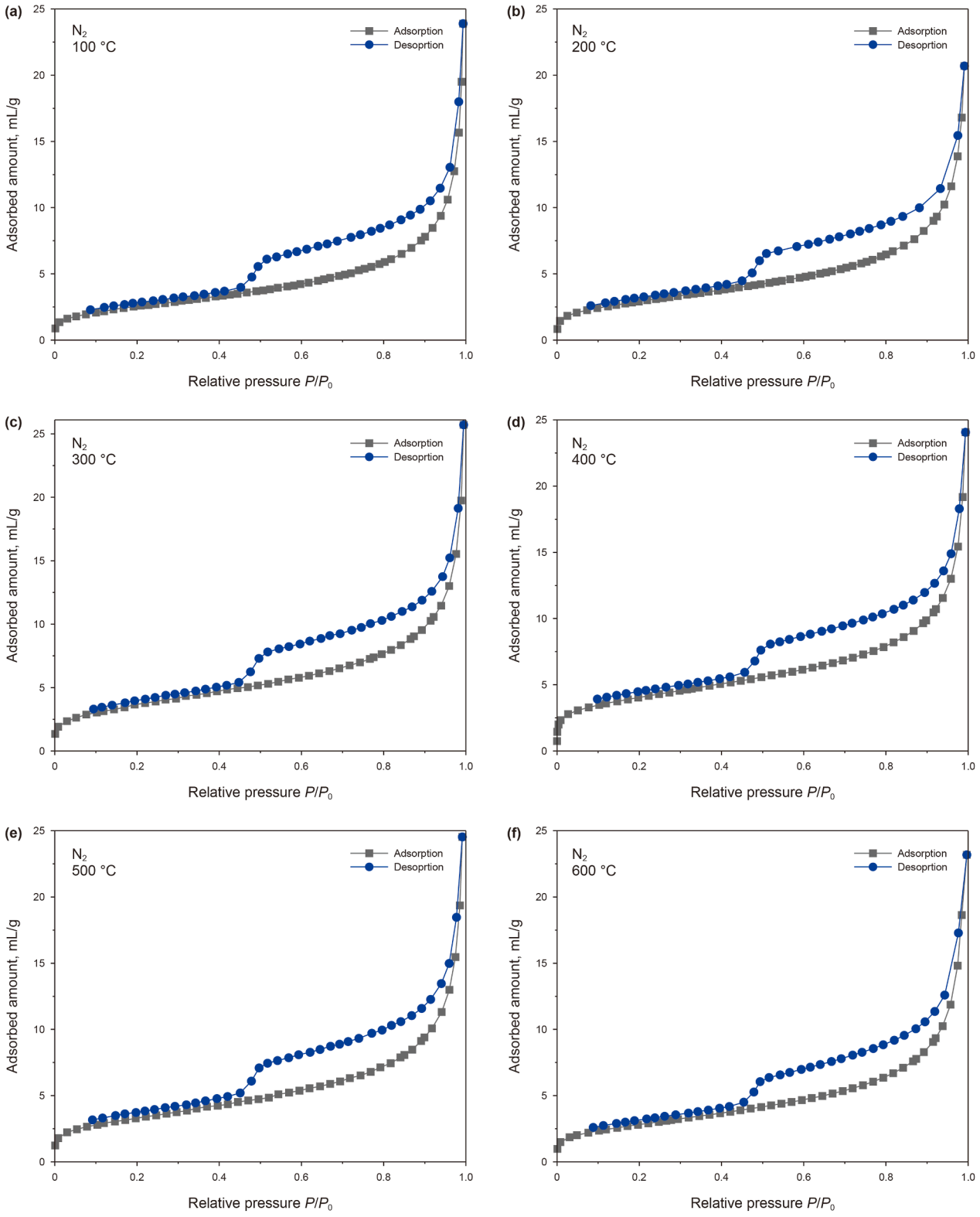

Fig. 8. N_2 adsorption–desorption curves of shale samples after pyrolysis at various temperatures under a N_2 atmosphere.

evaporation of free water, adsorbed water, and interlayer water in clay minerals, accompanied by partial desorption of adsorbed gases. At 300 °C, oil-phase products emerge but kerogen pyrolysis remains inefficient, predominantly forming unstable intermediate asphaltenes. Progressive heating to over 350 °C initiates gradual oil yield, which surges to 6.34% at 450 °C and peaks at 11.96% by 500 °C. This maximum yield is attributed to thermally enhanced kerogen cracking and development of abundant macropores within shale matrix facilitating pyrolytic oil expulsion. However, further temperature elevation to 550 °C reduces oil yield due to

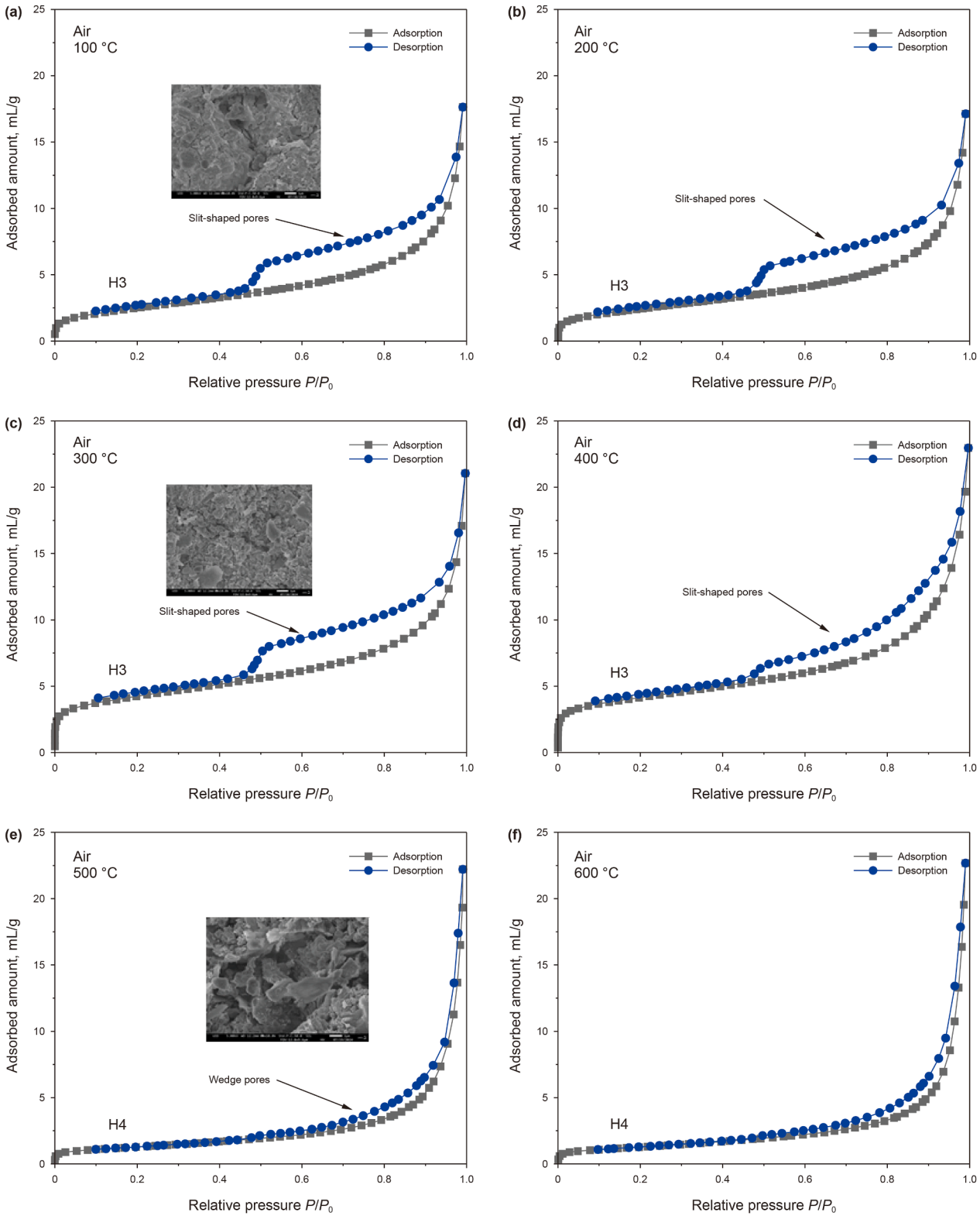

Fig. 9. N_2 adsorption–desorption curves of shale samples after cracking at various temperatures at an air atmosphere.

secondary cracking of light oil components into gaseous hydrocarbons, thereby diminishing liquid production.

Under an oxygen-lean atmosphere (Fig. 12), the overall trend of oil yield from ambient to 550 °C resembles that observed in a N_2 atmosphere, exhibiting an initial rise followed by a decline. However, the peak oil yield occurs at a lower temperature compared to the nitrogen system. This phenomenon indicates that oxygen participation exerts a catalytic effect on kerogen cracking at medium-high temperatures, wherein oxidative consumption of residual carbon releases thermal energy that propagates inward

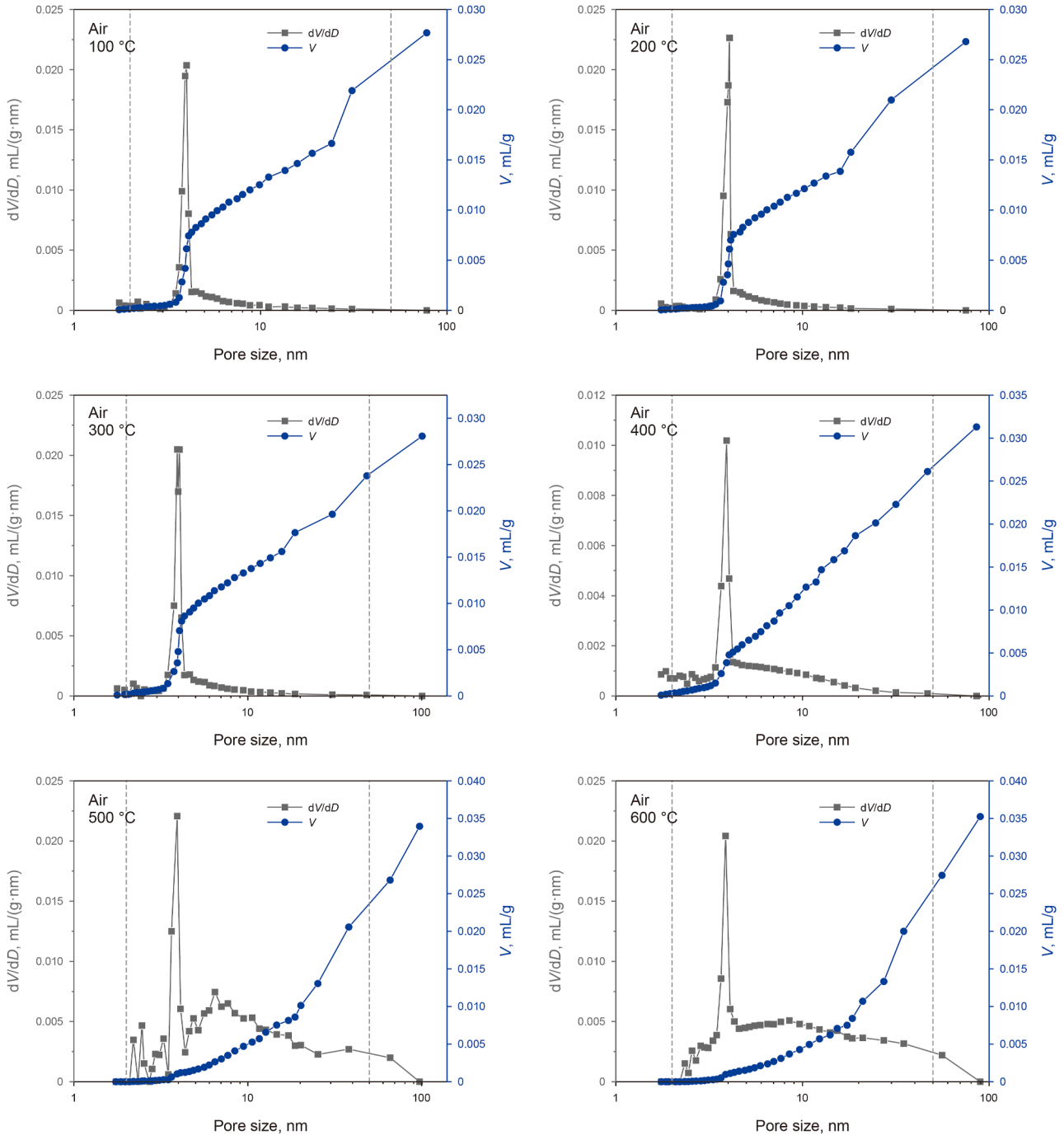

Fig. 10. Pore size evolution of shales at different temperatures under an air atmosphere.

Table 2
Shale oil yield rate by oxidative cracking in oxygen-reduced air.

Cracking temperature, °C	Initial weight, g	Weight after cracking, g	Weight loss, g	Loss percent, %	Oil weight, g	Oil yield, %
100	57.122	57.095	0.027	0.05	0	0
200	58.248	57.957	0.290	0.50	0	0
300	59.134	58.120	1.013	1.71	0.266	0.45
350	60.214	57.599	2.915	4.84	1.643	2.73
400	58.854	52.626	6.227	10.58	3.484	5.92
450	56.207	43.306	12.901	22.95	6.868	12.22
500	57.100	42.742	14.357	25.14	6.155	10.78
550	59.002	45.005	13.996	23.72	5.640	9.56

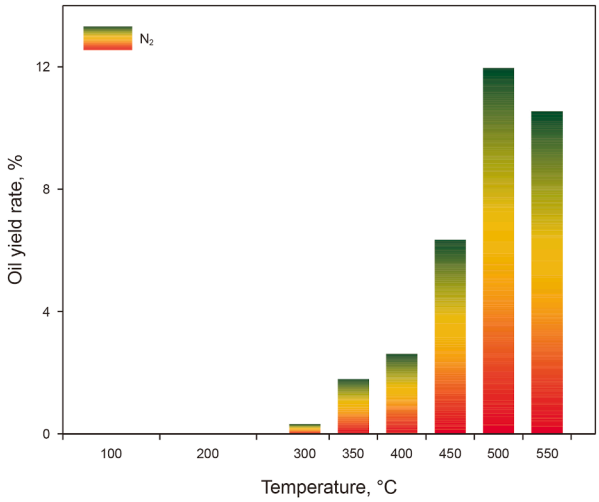

Fig. 11. Oil yield performance by N_2 pyrolysis at various temperatures.

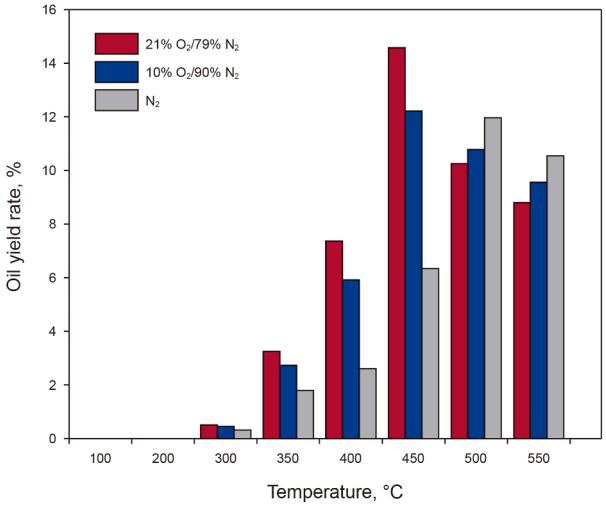

Fig. 13. Comparison of oil yields under three atmospheric cracking.

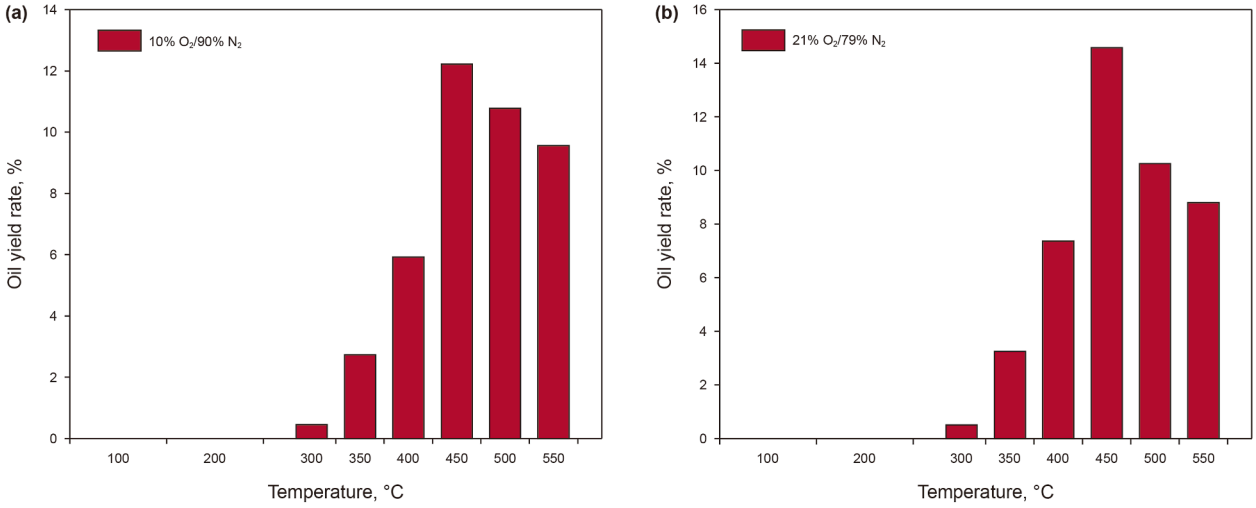

Fig. 12. Oil yield performance by 10% (**a**) and 21% (**b**) O_2 cracking.

through the organic-rich shale matrix, promoting large-scale kerogen cracking. Fig. 13 integrates comparative oil yield results under three different oxygen concentrations. Oxygen-containing atmospheres achieve peak yields about 450 °C, suggesting near-complete organic matter conversion. Beyond 450 °C, the oil yield decline correlates with secondary cracking and coking severity, both exhibiting positive correlation with oxygen concentration. Excessive oxygen and temperature induce over-oxidation and over-cracking, ultimately suppressing pyrolytic oil recovery efficiency.

4. Conclusions

(1) Integrated multiscale experiments reveal the mechanistic impacts of oxidative cracking on thermogravimetric behavior, mineralogical evolution, porosity response, and oil yield kinetics in organic-rich shales. It demonstrates technical advantages of oxidative atmospheres over conventional inert pyrolysis. Thermogravimetric analysis indicates pronounced exothermic characteristics within the core cracking interval (290–600 °C) under oxidative conditions, where oxygen participation accelerates organic matter cracking, shifting cracking toward lower temperatures, compared to inert atmospheres exhibiting suppressed reaction kinetics.

(2) Isothermal nitrogen adsorption–desorption experiments document substantial pore structure expansion under an air atmosphere. Upon exceeding 500 °C, pore morphology transitions from slit-shaped plate pores to open cylindrical configurations. Nuclear magnetic resonance (NMR) analyses further confirm that oxygen intervention in high-temperature air atmospheres promotes oxidative consumption of residual carbon, liberating nascent pore space while enhancing cracking kinetics through accelerated expansion, interconnection, and coalescence of meso and macropores.

Collectively, oxygen introduction drives cracking advancement by reducing the temperature threshold for kerogen cracking by approximately 50 °C, achieving maximum oil yield at 450 °C. This paradigm shift demonstrates the thermodynamic superiority of

controlled oxidative environments in unlocking unconventional hydrocarbon resources.

CRediT authorship contribution statement

Tao Wan: Writing – original draft, Methodology, Funding acquisition. **Xiao Zhang:** Writing – original draft. **Ji-Xiang He:** Supervision, Project administration. **Yan Dong:** Validation, Supervision, Project administration.

Declaration of competing interest

The authors declare that they have no known competing financial interests or personal relationships that could have appeared to influence the work reported in this paper.

Acknowledgements

This work was support from NSFC (52564005 and 52574068), Xinjiang Tianshan Innovation Team (2024D14004) and Xinjiang Tianshan Talent Training Program (2023TSYCJC0002).

References

Bai, F., Sun, Y., Liu, Y., et al., 2017. Evaluation of the porous structure of Huadian oil shale during pyrolysis using multiple approaches. Fuel 187, 1–8. https://doi.org/10.1016/j.fuel.2016.09.012.

Bai, J., Wang, Q., Jiao, G., 2012. Study on the pore structure of oil shale during low-temperature pyrolysis. Energy Proc. 17, 1689–1696. https://doi.org/10.1016/j.egypro.2012.02.299.

Boyabat, N., Ozer, A.K., Bayrakçeken, S., et al., 2004. Thermal decomposition of pyrite in the nitrogen atmosphere. Fuel Process. Technol. 85 (2–3), 179–188. https://doi.org/10.1016/S0378-3820(03)00196-6.

Chen, S., Zuo, Z., Moore, T.A., et al., 2018. Nanoscale pore changes in a marine shale: A case study using pyrolysis experiments and nitrogen adsorption. Energy Fuels 32 (9), 9020–9032. https://doi.org/10.1021/acs.energyfuels.8b01405.

Dunn, J.G., De, G.C., O'Connor, B.H., 1989. The effect of experimental variables on the mechanism of the oxidation of pyrite: Part 1. Oxidation of particles less than 45 μm in size. Thermochim. Acta 145, 115–130. https://doi.org/10.1016/0040-6031(89)85131-7.

Fang, C., Li, S., Ma, G., et al., 2012. Reaction mechanism and kinetics of pressurized pyrolysis of Chinese oil shale in the presence of water. Pet. Sci. 9, 532–534. https://doi.org/10.1007/s12182-012-0239-0.

Gai, R., Jin, L., Zhang, J., et al., 2014. Effect of inherent and additional pyrite on the pyrolysis behavior of oil shale. J. Anal. Appl. Pyrolysis 105, 342–347. https://doi.org/10.1016/j.jaap.2013.11.022.

Gao, Y., Wan, T., Dong, Y., et al., 2022. Numerical and experimental investigation of production performance of in-situ conversion of shale oil by air injection. Energy Rep. 8, 15740–15753. https://doi.org/10.1016/j.egyr.2023.01.119.

Gao, Z., Fan, Y., Xuan, Q., et al., 2020. A review of shale pore structure evolution characteristics with increasing thermal maturities. Adv. Geo-Energy Res. 4 (3), 247–259. https://doi.org/10.46690/ager.2020.03.03.

Geng, Y., Liang, W., Liu, J., et al., 2017. Evolution of pore and fracture structure of oil shale under high temperature and high pressure. Energy Fuels 31 (10), 10404–10413. https://doi.org/10.1021/acs.energyfuels.7b01071.

Guan, M., Liu, X., Jin, Z., et al., 2022. The evolution of pore structure heterogeneity during thermal maturation in lacustrine shale pyrolysis. J. Anal. Appl. Pyrolysis 163, 105501. https://doi.org/10.1016/j.jaap.2022.105501.

Guo, Y., Huang, L., Li, X., et al., 2020. Experimental investigation on the effects of thermal treatment on the physical and mechanical properties of shale. J. Nat. Gas Sci. Eng. 82, 103496. https://doi.org/10.1016/j.jngse.2020.103496.

Han, X., Jiang, X., Yu, L., et al., 2006. Change of pore structure of oil shale particles during combustion. Part 1. Evolution mechanism. Energy Fuels 20 (6), 2408–2412. https://doi.org/10.1021/ef0603277.

Hao, N., Ben, H., Yoo, C.G., et al., 2016. Review of NMR characterization of pyrolysis oils. Energy Fuels 30 (9), 6863–6880. https://doi.org/10.1021/acs.energyfuels.6b01002.

Hu, G., Dam-Johansen, K., Wedel, S., et al., 2006. Decomposition and oxidation of pyrite. Prog. Energy Combust. Sci. 32 (3), 295–314. https://doi.org/10.1016/j.pecs.2005.11.004.

Ifticene, M.A., Yuan, C., Al-Muntaser, A.A., et al., 2022. Behavior and kinetics of the conversion/combustion of oil shale and its components under air condition. Fuel 324, 124597. https://doi.org/10.1016/j.fuel.2022.124597.

Jiang, C., Xu, L., Chen, Y., et al., 2024. Thermal behavior of minerals in shale and its influence on evolution of gas-flow channels under thermal shock. Gas Sci. Eng. 121, 205183. https://doi.org/10.1016/j.jgsce.2023.205183.

Lei, J., Pan, B., Guo, Y., et al., 2021. A comprehensive analysis of the pyrolysis effects on oil shale pore structures at multiscale using different measurement methods. Energy 227, 120359. https://doi.org/10.1016/j.energy.2021.120359.

Li, P.S., Chen, M.J., Kang, Y.L., et al., 2023. Multiscale pore structural alteration in gas shale by supercritical water stimulation. Geoenergy Sci. Eng. 229, 212106. https://doi.org/10.1016/j.geoen.2023.212106.

Liu, B., Yao, C., Qi, J., et al., 2024. Experimental investigation on pyrolysis products and pore structure characteristics of organic-rich shale heated by supercritical carbon dioxide. Pet. Sci. 21 (4), 2393–2406. https://doi.org/10.1016/j.petsci.2024.01.022.

Liu, Z., Ma, H., Guo, J., et al., 2022. Pyrolysis characteristics and effect on pore structure of Jimsar oil shale based on TG-FTIR-MS analysis. Geofluids 2022, 7857239. https://doi.org/10.1155/2022/7857239.

Meng, F., Yao, C., Du, X.W., et al., 2023. Experimental investigation on composition and pore structure evolution of organic-rich shale via supercritical water. Energy Fuels 37 (17), 15671–15686. https://doi.org/10.1021/acs.energyfuels.3c02441.

Meng, F., Yao, C., Yang, H., et al., 2024. Changes of the multiscale pore structure and connectivity of organic-rich shale during hydrous pyrolysis under different temperatures and pressures. Energy Fuels 38 (18), 17554–17570. https://doi.org/10.1021/acs.energyfuels.4c02149.

Pan, Y., Li, M., Sun, Y., et al., 2023. Characterization of free and bound bitumen fractions in a thermal maturation shale sequence. Part 2: Structural evolution of kerogen and bitumen during shale oil generation, expulsion and retention. Org. Geochem. 182, 104640. https://doi.org/10.1016/j.orggeochem.2023.104640.

Rabbani, A., Baychev, T.G., Ayatollahi, S., et al., 2017. Evolution of pore-scale morphology of oil shale during pyrolysis: A quantitative analysis. Transport Porous Media 119, 143–162. https://doi.org/10.1007/s11242-017-0877-1.

Saif, T., Lin, Q., Bijeljic, B., et al., 2017. Microstructural imaging and characterization of oil shale before and after pyrolysis. Fuel 197, 562–574. https://doi.org/10.1016/j.fuel.2017.02.030.

Shi, Y., Weng, D., Cai, B., et al., 2024. Flow and heat transfer of shale oil reservoir during CO_2 enhanced pyrolysis: A pore-scale modeling. Processes 12 (8), 1694. https://doi.org/10.3390/pr12081694.

Sing, K.S.W., Everett, D.H., Haul, R.A.W., Moscou, L., Pierotti, R.A., Rouquerol, J., 1985. Reporting physisorption data for gas/solid systems with special reference to the determination of surface area and porosity. Pure Appl. Chem. 57, 603–619.

Sun, J., Xiao, X., Cheng, P., et al., 2019. Formation and evolution of nanopores in shales and its impact on retained oil during oil generation and expulsion based on pyrolysis experiments. J. Petrol. Sci. Eng. 176, 509–520. https://doi.org/10.1016/j.petrol.2019.01.071.

Tang, J., Honghao, Y., Xiao, Z., et al., 2025. Influence of pyrolysis degree on oil shale anisotropy and damage deterioration characteristics. Rock Mech. Rock Eng. 58 (1), 965–980. https://doi.org/10.1007/s00603-024-04197-7.

Tiwari, P., Deo, M., Lin, C.L., et al., 2013. Characterization of oil shale pore structure before and after pyrolysis by using X-ray micro CT. Fuel 107, 547–554. https://doi.org/10.1016/j.fuel.2013.01.006.

Wang, L., Yang, D., Kang, Z., et al., 2022. Experimental study on the effects of steam temperature on the pore-fracture evolution of oil shale exposed to the convection heating. J. Anal. Appl. Pyrolysis 164, 105533. https://doi.org/10.1016/j.jaap.2022.105533.

Wang, L., Zhao, Y., Yang, D., et al., 2019. Effect of pyrolysis on oil shale using superheated steam: A case study on the Fushun oil shale, China. Fuel 253, 1490–1498. https://doi.org/10.1016/j.fuel.2019.05.134.

Wang, Q., Ye, J., Yang, H., et al., 2016. Chemical composition and structural characteristics of oil shales and their kerogens using fourier transform infrared (FTIR) spectroscopy and solid-state ^{13}C nuclear magnetic resonance (NMR). Energy Fuels 30 (8), 6271–6280. https://doi.org/10.1021/acs.energyfuels.6b00770.

Xu, S., Sun, Y., Lü, X., et al., 2021. Effects of composition and pore evolution on thermophysical properties of Huadian oil shale in retorting and oxidizing pyrolysis. Fuel 305, 121565. https://doi.org/10.1016/j.fuel.2021.121565.

Yang, D., Wang, L., Zhao, Y., et al., 2021. Investigating pilot test of oil shale pyrolysis and oil and gas upgrading by water vapor injection. J. Petrol. Sci. Eng. 196, 108101. https://doi.org/10.1016/j.petrol.2020.108101.

Yang, L., Yang, D., Zhao, J., et al., 2016. Changes of oil shale pore structure and permeability at different temperatures. Oil Shale 33 (2), 101. https://doi.org/10.3176/oil.2016.2.01.

Zhan, H., Qin, F., Chen, S., et al., 2022. Two-step pyrolysis degradation mechanism of oil shale through comprehensive analysis of pyrolysis semi-cokes and pyrolytic gases. Energy 241, 122871. https://doi.org/10.1016/j.energy.2021.122871.

Zhang, X., Guo, W., Pan, J., et al., 2024. In-situ pyrolysis of oil shale in pressured semi-closed system: Insights into products characteristics and pyrolysis mechanism. Energy 286, 129608. https://doi.org/10.1016/j.energy.2023.129608.

Zhao, F., Yang, Z., Zhang, L., et al., 2025. The effect of temperature on pyrolysis products during oil shale thermal decomposition. Sci. Rep. 15 (1), 26135. https://doi.org/10.1038/s41598-025-11050-6.

Zhao, J., Yang, L., Yang, D., et al., 2022. Study on pore and fracture evolution characteristics of oil shale pyrolysed by high-temperature water vapour. Oil Shale 39 (1), 79–95. https://doi.org/10.3176/oil.2022.1.05.

Zhao, S., Sun, Y., Lu, X., et al., 2020. Energy consumption and product release characteristics evaluation of oil shale non-isothermal pyrolysis based on TG-DSC. J. Petrol. Sci. Eng. 187, 106812. https://doi.org/10.1016/j.petrol.2019.106812.